UNIVERSITY OF
BATH

Citation for published version:
Fraser, K & Poelma, C 2013, 'Enhancing the dynamic range of Ultrasound Imaging Velocimetry using interleaved imaging' Paper presented at International Symposium on Particle Image Velocimetry, Delft, Netherlands, 1/07/13 - 3/07/13, .

Publication date:
2013

Link to publication

University of Bath

Enhancing the dynamic range of Ultrasound Imaging Velocimetry using interleaved imaging

C. Poelma[1] and K. H. Fraser[2]

[1] Laboratory for Aero & Hydrodynamics (3ME-P&E), Delft University of Technology, Leeghwaterstraat 21, 2628 CA Delft, The Netherlands

[2] Department of Bioengineering, Imperial College London, South Kensington Campus, SW7 2AZ London, United Kingdom

ABSTRACT

In recent years, non-invasive velocity field measurement based on correlation of ultrasound images has been introduced as a promising technique for fundamental research into disease processes, as well as a diagnostic tool. A major drawback of the method is the relatively limited dynamic range when conventional echography equipment is used. We present a method by which the restriction of the maximum flow rates can be relaxed. The method uses conventional hardware, but a novel read-out sequence that interleaves subsequent images. By varying the off-set between two interleaved images, we re-introduce the inter-frame time as a parameter that can be optimized for velocimetry. The novel approach is demonstrated with data from an in vitro study of a reference flow.

1. Introduction

There is a significant research effort to improve the *in vivo* measurement of blood flow patterns (Taylor and Draney 2004, Van Ooij et al. 2012, Hoskins 2010). Better knowledge of hemodynamic conditions will assist in fundamental studies of the role of hemodynamics in pathologies, e.g. the development of aneurysms or atherosclerosis. Furthermore, a robust measurement technique can be an important diagnostic tool for clinical screening and post-operative monitoring. Naturally, non-invasive techniques with sufficient spatial resolution are desirable. The resolution requirement is particularly important if the wall shear stress distribution in a complex geometry needs to be determined and knowledge of just the mean flow is insufficient. In recent years, ultrasound imaging velocimetry - also known as 'echo-PIV' (Kim et al. 2004, Zheng et al. 2006, Beulen et al. 2010, Poelma et al. 2011b), as the processing is done using conventional Particle Image Velocimetry tools - has been introduced as a technique that can provide the desired blood flow patterns non-invasively (Sengupta et al. 2007, Hong et al. 2008, Kheradvar et al. 2011, Zhang et al. 2011, Poelma et al. 2012). As it is largely based on established echography hardware and protocols, it is an accessible and relatively cheap method. The method uses cross-correlation algorithms to track features in subsequent frames of an image sequence. In contrast to *Doppler* velocimetry, it provides instantaneous velocity fields of *two* velocity components, without the drawbacks associated with insonification angle inaccuracies.

A significant drawback at the moment is the limited dynamic velocity range of the technique: current hardware and acquisition strategies lead to a limit of the acquisition of typically hundreds of images per second. This leads, as shown in the next section, to an upper limit of the flow velocities that can be acquired. This limit is often well within the range of blood flow velocities that are encountered in both the (diseased) human circulatory system and animal studies. In this study, we present a novel acquisition strategy that effectively eliminates the upper limit. We do this by acquiring images in an interleaved[1] manner, where two subsequent frames are not recorded in series, but in an alternating manner. While this reduces the temporal resolution by a factor of two, the velocity dynamic range can be extended dramatically. Note that the reduced measurement rate (i.e. the number of velocity fields per second that becomes available) is still sufficient to study rapid transient blood flow phenomena. We demonstrate the technique in an vitro reference flow and show that much higher flow rates are now within reach with current hardware.

2. Background

Before introducing the novel approach, the standard practice in ultrasound imaging velocimetry is first briefly reviewed, which also introduces the terminology, coordinate systems and definitions. While some descriptions may initially appear superfluous in the conventional method, they will be very helpful in the explanation of the interlaced method.

---

[1]We here use the term 'interleaved' to distinguish the method from the more conventional 'interlaced' imaging, where the apparent frame rate is doubled by reading out even or odd lines in an alternating manner.
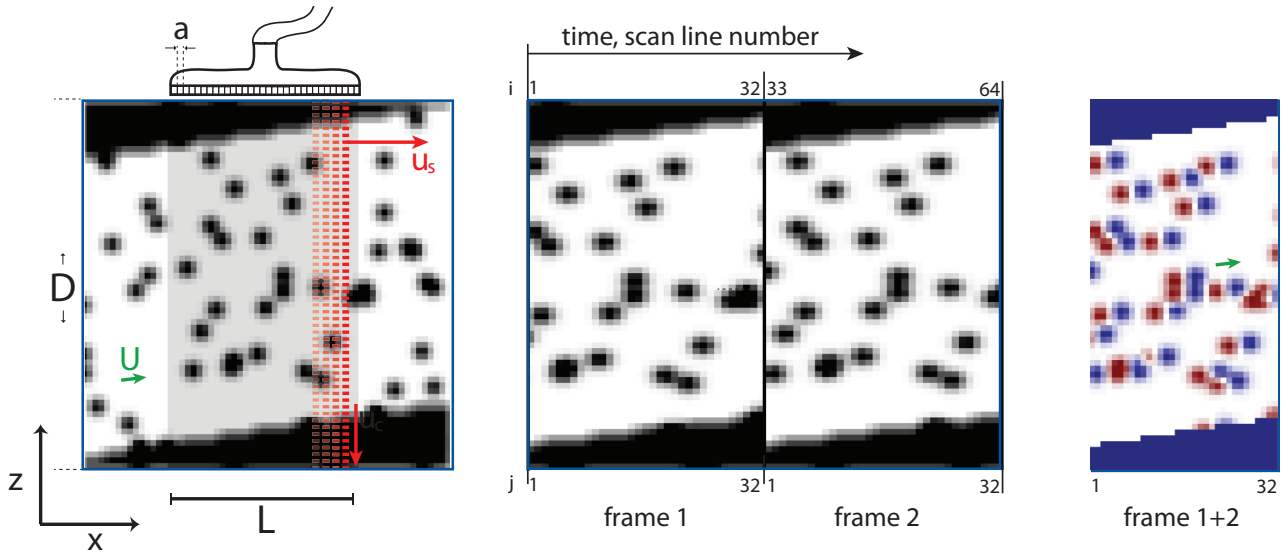
Figure 1: Schematic representation of the ultrasound imaging velocimetry method. (*left*): the region of interest with coordinate system. The region of interest is scanned line-by-line. (*middle*) Two frames that are recorded subsequently. (*right*) Superposition of the two frames (red is first frame, blue is second frame).

2.1 Imaging and terminology

In figure 1, a schematic representation of ultrasound imaging is shown as used for velocimetry measurements. The left-hand panel shows how a region of interest is imaged by placing a linear transducer, which axis is aligned with the main flow direction; here the flow is predominantly in the positive x direction, with a velocity of U. The flow contains tracers, e.g. in the form of contrast medium, see experimental section. Rather than acquire snapshots (as cameras do in conventional PIV), the transducer elements are read out *sequentially* to form one image ('rolling shutter' imaging). Note that for simplicity, we here use 'images' to describe the data that is received by the transducers. The same reasoning holds for the actual radiofrequency data, B-mode images, harmonic imaging, etc. In the case shown in the middle figure, the image is swept in the direction of the flow. The time to record a vertical line of an image by one transducer elements depends on the depth of the image (D; a parameter specified during measurements) and the speed of sound, c. The transit time, i.e. the time between sending an ultrasound pulse and receiving an echo, is approximately $\tau \approx 2D/c$. For a typical depth of $D = 10$ *cm* and a speed of sound of 1500 m/s (Hill et al. 2004), recording a single line requires approximately 0.13 *ms*; this implies that $f = 1/\tau$ lines per second can be obtained (ignoring any overhead or bandwidth limitations in the electronics). For a given pitch between elements (a), the sweep velocity can be calculated: $u_s \equiv a/\tau$. For very high sweep velocities, the resulting images can be considered to be instantaneous snapshots. For lower sweep velocities, the images of moving tracers are either compressed or stretched, depending on the direction of the read-out. For extreme cases, $U \geq u_s$, no meaningful images can be obtained (tracer particles would appear as horizontal lines for $U = u_s$). The sweep velocity has units of velocity (m/s), but sometimes it is more convenient to express it as lines-per-second (s^{-1}). We will use u'_s in this case, which is defined as $u'_s \equiv u_s/a$. Note that this is identical to the frequency f that was introduced earlier, but u'_s also contains a direction in its sign.

In the middle panel of figure 1, the result of two subsequent sweeps (i.e. sequential read-outs of the transducer elements) are shown. In this case, the image consists of 32 vertical lines; the index j refers to the transducer element and corresponding column in the image. The index i refers to the sequence of the data, i.e. equivalent to the read-out time step. In this straightforward case, element $j = 1 \cdots 32$ are read-out during time steps $i = 1 \cdots 32$. Once the complete image has been recorded, the process is repeated. This leads to a new image (denoted 'frame 2'), again consisting of line $j = 1 \cdots 32$, this time read-out at time-steps $i = 33 \cdots 64$. The right-hand panel of figure 1 shows the superposition of the two recorded images.

The total time needed to record a single image is $T = nf$, with n the number of elements or columns in the image. Alternatively, it can be found by dividing the width of the image L by the sweep velocity, $T = L/u_s$. This is the time between subsequent images and thus serves as inter-frame time ΔT for conventional ultrasound imaging velocimetry. As will be discussed later, this is a critical parameter in the performance of the correlation algorithm.

2.2 PIV processing

Once two subsequent image frames are recorded - usually as part of a whole series, the local displacement of tracer particle images can be determined. As in standard Particle Image Velocimetry, this is done using cross-correlation of smaller subsets of the image, so-called interrogation areas (Adrian and Westerweel 2010). Figure 2 summarizes the correlation process in a schematic manner. The entire image is divided in smaller windows (typically of 8×8 to 64×64 pixels, depending on the imaging and flow conditions. The interrogation areas are cross-correlated with their equivalent areas in the subsequent frame. The maximum in the correlation plane corresponds to the most likely displacement of the tracer particle pattern (as long as there is a uniform motion of a sufficient amount of tracer particles). Analyzing all interrogation areas produces a vector field that represents the local displacement field, which can be

frame 1+2　　　　　　　　correlation plane　　　　　　　　PIV result
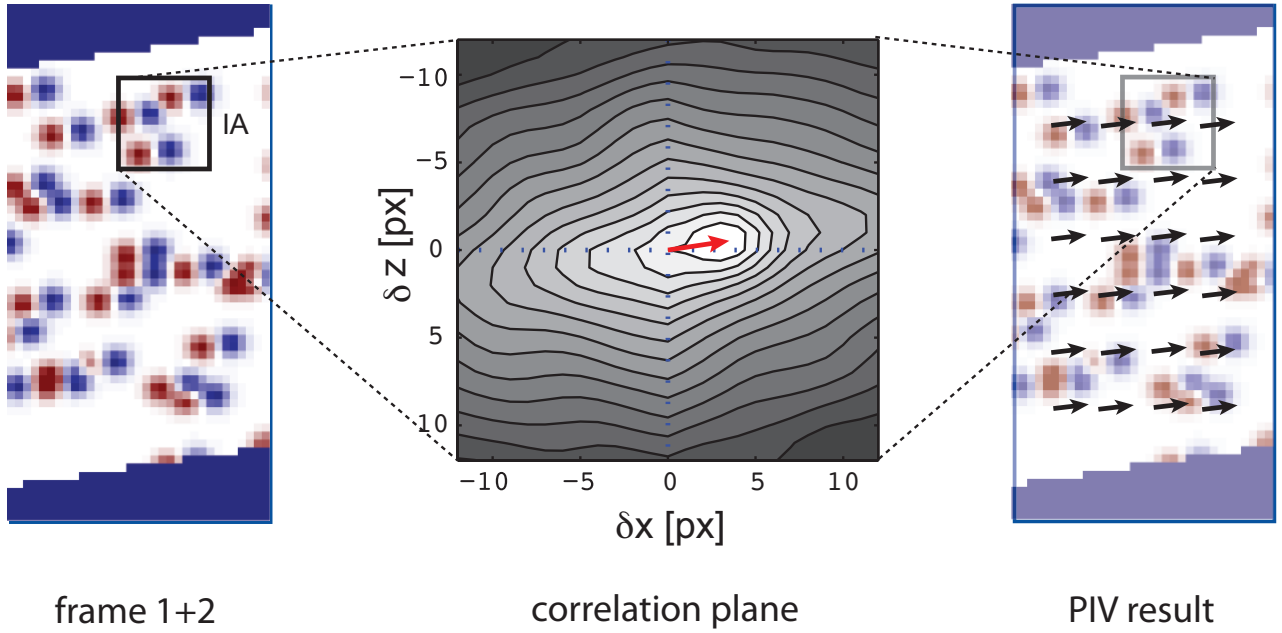
Figure 2: PIV processing of an image pair (shown *left*): the local cross-correlation result (*middle*) provides the most likely displacement within each interrogation area (IA). The final result is an instantaneous vector field (*right*).

translated into a velocity field. For conventional (optical) PIV applications, the displacements δ_x and δ_z are divided by the inter-frame time directly to obtain the velocity components ($u_x = C\delta_x/\Delta T$, $u_z = C\delta_z/\Delta T$); C is a calibration constant that converts from pixels to physical dimensions.

Due to the nature of the recording of ultrasound images, the conversion from pixel displacement to velocities is less straightforward: the lines of an image are not recorded at the same time, so the inter-frame time ΔT needs to be corrected for any displacement (Poelma et al. 2011b, Zhou et al. in print). Simply stated: a particle moving against the sweep direction effectively has a shorter inter-frame time than a particle moving with the sweep direction. For ultrasound PIV, the sweep-corrected velocities are given by:

$$u_x = C_x \frac{\delta_x}{\Delta T + \delta_x/u_s'} \tag{1}$$

$$u_z = C_z \frac{\delta_z}{\Delta T + \delta_x/u_s'} \tag{2}$$

In these equations, the sign of the terms $\delta_{x,z}$ and u_s' is relevant: the correction is different for sweeping against or with the flow direction. The two scaling coefficients C_x and C_z generally have different values; the former is determined by the transducer pitch (*a*), while the latter is determined by the speed of sound and transducer sampling methods. Notice also that the denominator of equation 2 also contains the 'horizontal' displacement δ_x: a vertical displacement (i.e. along the axis of the propagation of sound) does not require a correction for PIV analysis, yet vertical velocities need to be corrected if there is a local horizontal displacement.

The inter-frame delay time ΔT is a critical parameter in the optimization of PIV measurements. As the velocity is usually fixed by the problem under investigation, the value of ΔT determines the displacement δ of tracer particle images between subsequent frames (recall that displacement is proportional to velocity multiplied by ΔT). When displacements are too small, the results will be unacceptably noisy. This is caused by the finite error that exists when the location of the displacement peak is determined. This error should be small compared to the actual displacement. However, for values of ΔT that are too large, the particles will leave the interrogation area. The height of the displacement peak - and thus the chance of obtaining a good displacement estimate - decreases linearly with increasing displacement; the so-called 'loss-of-pair' coefficient for in-plane motion (N_i) is given as (Adrian and Westerweel 2010):

$$N_i = 1 - \frac{|\delta_x|}{l_x} \qquad |\delta_x| < l_x \tag{3}$$

$$N_i = 0 \qquad |\delta_x| \geq l_x \tag{4}$$

Here l_x is the size (in pixels) of the interrogation area; as is evident from the equations (and confirmed by simple reasoning) it is not possible to successfully measure a displacement that is larger than an interrogation area: all particles will leave the domain and the

cross-correlation will only contain noise peaks. In practice, measurements are designed so that the displacements are up to a quarter of the interrogation area size, the so-called 'quarter rule', Adrian and Westerweel (2010). This heuristic rule aims to find an optimum between the two aforementioned noise sources (peak location error, loss-of-pair).

2.3 Dynamic range limitations

Note that in conventional PIV, the inter-frame time ΔT is a parameter that can be freely chosen, as most applications make use of dual-cavity pulsed lasers and interline transfer CCD cameras that can recorded two images within rapid succession. In ultrasound-based velocimetry, this is not the case: the inter-frame time is determined by the acquisition rate of the system, $\Delta T = T$, ignoring the corrections mentioned in equation 1 and 2 for simplicity. Furthermore, in ultrasound imaging we cannot change the magnification easily, so that optimization of the displacement for a given velocity using the calibration/scaling constant C is also impossible.

This feature of ultrasound imaging velocimetry directly leads to an upper limit of the velocity that can be measured. One could argue that larger interrogation areas could be used, even up to the full width of the image (Beulen et al. 2010). However, this limits the transverse (x) resolution. Alternatively, iterative methods can be used, e.g. based on local window shifting, that circumvent the quarter-rule (Adrian and Westerweel 2010). However, if the flow has an out-of-plane component, either due to a misalignment of the transducer with the flow direction or due to secondary flow or turbulence, tracer particles will still leave the observation domain for larger inter-frame times and meaningful results cannot be obtained.

This upper limit is widely reported in the literature as a major problem. For example, Kheradvar et al. (2010) report a velocity cut-off at 30 cm/s at an imaging rate of 35 fps and 70 cm/s at 80 fps. Using specialized hardware, Zhang et al. (2011) describe preliminary in vivo results using acquisitions in the 500-700 fps range. They managed to measure the flow in a carotid artery of a healthy volunteer (70-80 cm/s). However, they point out that in diseased vessels the required velocity dynamic range likely needs to be higher. Westerdale et al. (2011) obtained peak velocities of 30 cm/s at 60 frames per second. Poelma et al. (2012) report a maximum velocity (70 cm/s, in vitro) and also study the effect of the acquisition rate (i.e. the number of elements used) on the accuracy of flow measurements. Such a reduction of elements is a common approach to increase the imaging rate (since $T = n/f$). This can be done by restricting the field-of-view or by skipping lines (at the cost of spatial resolution). With a strongly limited range of elements, the method effectively reduces to a single profile velocimetry method. For instance, Beulen et al. (2010) used only 14 transducer lines to obtain an image acquisition rate of 730 fps. This allowed them to measure profiles with a maximum velocity of 140 cm/s. However, the strength of ultrasound imaging velocimetry - the ability to instantaneously capture e.g. disturbed flow patterns in a 2D image - is then obviously lost. Note that there is no clear relationship between the reported framerates and the maximum velocity that could be measured: this depends on the pitch of the transducer, but also on flow characteristics such as the turbulence level or the amount of out-of-plane motion. Furthermore, imaging characteristics (contrast medium, image quality) and the software used may have an influence. For a more thorough analysis, including typical values of the quantities involved, one is referred to Poelma et al. (2012).

An alternative method to increase the imaging rate is to make use of so-called plane wave imaging (Montaldo et al. 2009). This has the drawback that it requires more expensive hardware and complicated post-processing and reduces the image quality. Finally, it should be mentioned that increasing frame rates toward the kHz range usually leads to storage issues and often only few seconds of RF data (and thus a limited number of cardiac cycles) can be stored in memory. This limits the use of phase-averaging of the quasi-steady flow fields, which can greatly enhance the signal-to-noise ratio (Poelma et al. 2008).
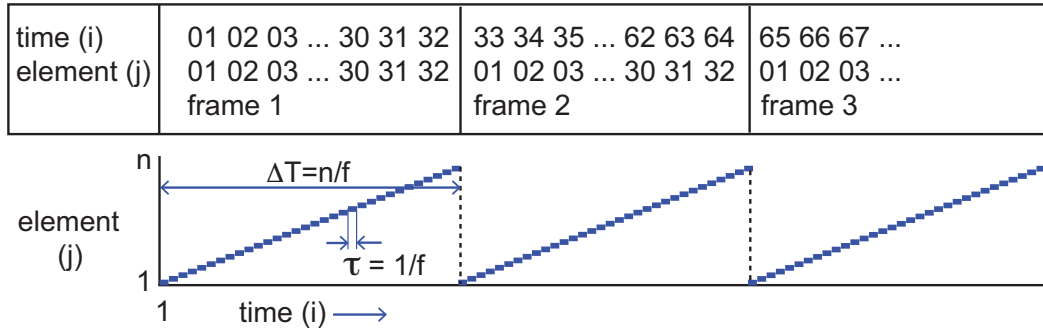
3. Interleaved Imaging

To circumvent the limitation of the maximum velocity that can be recorded, we here introduce a novel imaging method. This method relies on an acquisition strategy that is optimized for velocimetry, rather than imaging.
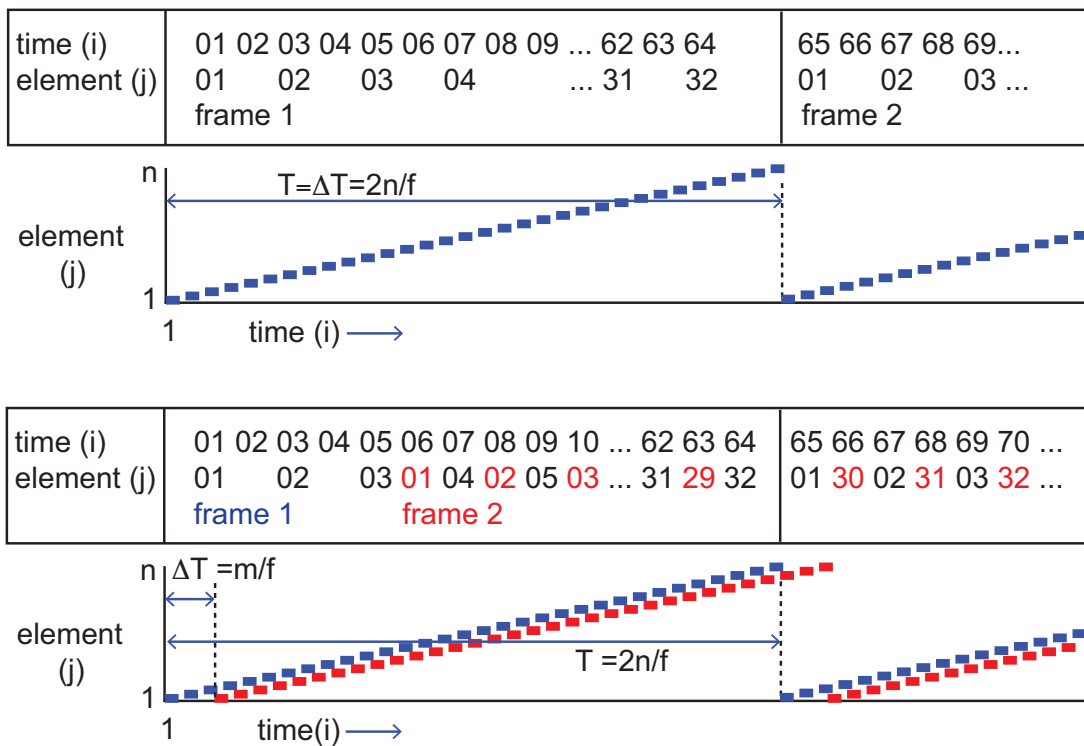
To introduce the method, we first describe the conventional 'sweeping' recording that is currently used. A schematic diagram is shown in figure 3. The diagram shows the time step (i) and element number (j), both in table form and in a graph. We here assume that the total number of elements (i.e. width of the image, n) is 32. The conventional imaging mode can be represented by a sawtooth-like graph: after recording line $j = n$ at timestep $i = n$, the next frame is recorded, starting at $i = n+1$ and $j = 1$. The effective ΔT, i.e. the time between recording the same region in subsequent images, is n/f (or τn) in this case.

In the new approach, we first record an image using utilizing only the odd time steps ($i = 1, 3, \cdots$); see the upper panel of figure 4: element j is recorded at timestep $i = 2j - 1$. Note that this effectively doubles the time required to recorded an image ($T = 2n/f$). However, we can now use the even time steps ($i = 2, 4, \cdots$) to record a second image. The second frame is shown in red in the timing diagram (bottom panel). The exact moment when the second frame will be recorded can be chosen freely; here we start recording it at time step $i = 6$. This gives us an effective $\Delta T = mf$, with m the number of steps between the start of the acquisition of frame 1 and the start of frame 2 - here $m = 5$. This re-introduces the critical inter-frame time into ultrasound-based PIV, as it is no longer linked to the image acquisition rate (T). The theoretical lower limit of ΔT is now $1/f$ for $m = 1$, i.e. a line is read out twice at the same spatial position before moving on the next line.

The acquisition frequency for each image *pair* is the same, although the time needed for one image is doubled. This means that the snapshot assumption (i.e. the total image is recorded at the same time) is even less appropriate than in normal ultrasound imaging.

time (i)	01 02 03 ... 30 31 32	33 34 35 ... 62 63 64	65 66 67 ...
element (j)	01 02 03 ... 30 31 32	01 02 03 ... 30 31 32	01 02 03 ...
	frame 1	frame 2	frame 3

Figure 3: Timing diagram for conventional ultrasound imaging. The effective ΔT, i.e. the time between recording the same region in subsequent images, is n/f.

time (i)	01 02 03 04 05 06 07 08 09 ... 62 63 64	65 66 67 68 69...
element (j)	01 02 03 04 ... 31 32	01 02 03 ...
	frame 1	frame 2

time (i)	01 02 03 04 05 06 07 08 09 10 ... 62 63 64	65 66 67 68 69 70 ...
element (j)	01 02 03 01 04 02 05 03 ... 31 29 32	01 30 02 31 03 32 ...
	frame 1 frame 2	

Figure 4: Timing diagram for interleaved imaging. Here an effective ΔT of 5τ is obtained by using an off-set $m = 5$.

interleaved image   de-interleaved   superposition
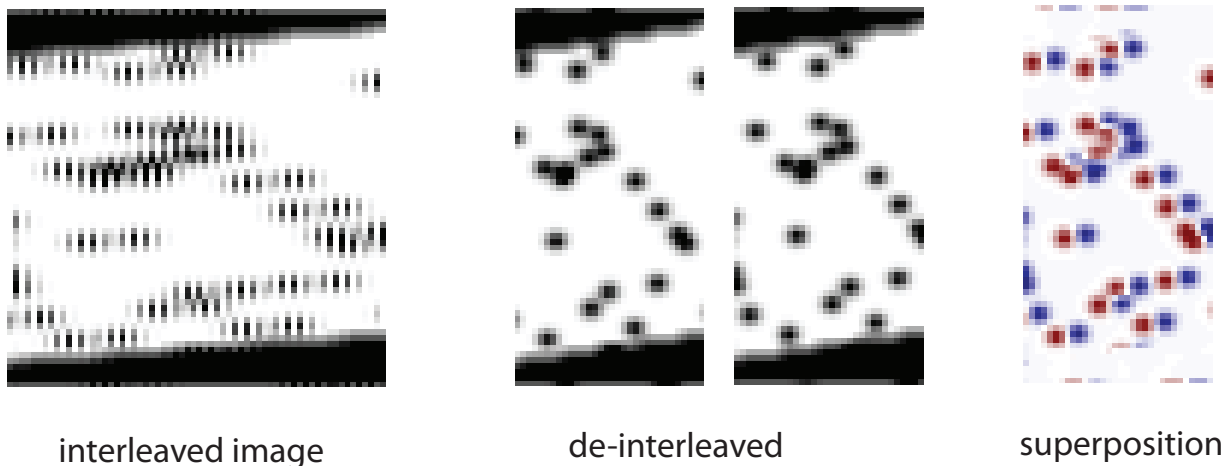
Figure 5: Schematic representation of interleaved imaging method: an interleaved image sequence that contains two frames. The separate frames can be obtained by de-interleaving them.

Correcting the displacements is also crucial in this case (equations 1 and 2). However, the effective acquisition rates are still in the hundreds of Hz range: acquisition is thus much faster than the time scales of typical cardiovascular flow, so the flow fields can still be assumed to be 'frozen'.

Figure 5 schematically shows an image sequence as it is recorded by the interleaved timing diagram shown in figure 4. An image pair is recorded using alternating (even/odd) lines (*left panel*). The recording can be split - keeping in mind the offset m - into two de-interleaved images (*middle panel*). The superposition in the right-hand panel shows these two frames. Note that the displacement for a given velocity can now be optimized by varying m (and thus ΔT), so that conditions can be chosen close to the 'quarter-rule'.

4. In vitro test case

To demonstrate the novel approach, it is applied to a reference flow. We here use the same experimental facility and equipment as described in detail in earlier studies (Poelma et al. 2011b, Poelma et al. 2012, Zhou et al. in print).

A straight tube phantom was set up to produce Poiseulle flow. The flow facility consisted of a 5 *mm* internal diameter latex tube (Pipeline Industries) held straight at either end in a tank of water with an acoustic absorber on the bottom. The working fluid was a mixture of water and glycerol (30% by weight; relative density 1.07 and dynamic viscosity 2.5 cP). Steady flow was produced by a centrifugal pump (EHEIM 1250A, Deizisau, Germany), and the flow rate was adjusted and measured using a resistor and rotameter respectively. The rotameter was validated before the experiments by measuring the outflow at constant discharge. The working fluid was seeding with SonoVue® contrast medium, which consists of 2-3 *μm* microbubbles of SF_6 gas.

An Ultrasonix RP500 scanner (Ultrasonix Medical Corporation, Canada), with a linear 128 element, 38 mm length, 5-14 MHz frequency, transducer (LP14-5/38) was used to obtain RF data. The transducer was positioned near the downstream end of the tube. This downstream position allowed for an entrance length of 50 cm (or 100 diameters), which ensures fully developed flow up to Reynolds numbers of 1600-1700. The transducer is clamped so as to produce an image of a longitudinal section at the midplane of the tube. The scanner was programmed using a Matlab interface to the Texo software development toolkit. This Matlab interface, developed by Dr. Jean Martial Mari, is available for download from the Ultrasonix Medical Corporation website (www.ultrasonix.com/wikisonix). Texo allows low level control of beam sequencing and RF data acquisition. A Matlab function was written which enabled the control of imaging parameters, including imaging depth D, number of lines n and interleave off-set m.

Ultrasound data was processed using a multi-pass PIV algorithm that uses image deformation and correlation averaging (Poelma et al. 2008). The analysis started with interrogation areas of 64×64 pixels and decreased to 8×8 pixels with 50% overlap for the final iterations. This corresponded to a spatial resolution of 1.2 mm by 0.09 mm in the x and z direction, respectively. Results were obtained by correlation-averaging of 100 image pairs. The chosen parameters may not be the most optimal if the ultimate goal was to determine the flow profile in the reference case (for instance, there is no variation in streamwise direction in this case, so the size of the interrogation areas could greatly be extended in that direction). However, we have chosen to fix the parameters - using values that would be useful in more complex geometries - in order to be able to compare the different cases. For the same reason, no vector validation (e.g. median test for outlier detection) or other post-processing steps were used.
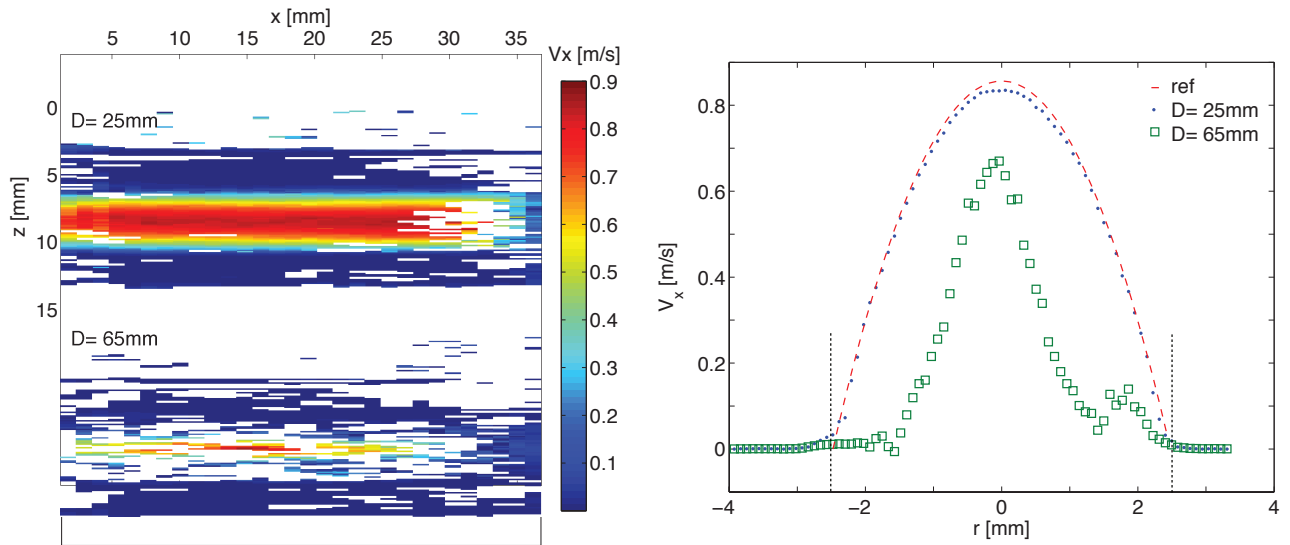
Figure 6: *(Left)* Contour plots of the velocity for two cases: $D = 25$ and 65 *mm*. Note that the bottom contour plot is shown with an arbitrary vertical off-set. *(Right)* Velocity profile for the two cases and the reference. The wall locations are indicated by the vertical dashed lines.

4.1 Conventional imaging

To demonstrate the limits of the dynamic velocity range we first report results using conventional ultrasound imaging velocimetry in figure 6. Two cases are shown, using an image depth (D) of 25 and 65 mm, respectively. The centerline velocity is kept constant at 0.86 m/s (Re = 920). The two depths result in frame rates of 140 and 72 Hz, or $\Delta T = 7.2$ ms and 13.8 ms, which in turn lead to centerline displacements of 25 and 46 pixels. The velocity component V_x is shown as two contour plots, with the case of $D = 65$ mm displaced with an arbitrary vertical off-set.

The measurement using $D = 25$ mm captures the flow field quite well: the centerline velocity is 2.5% less than the reference velocity (see also the right-hand side of figure 6). This discrepancy is within the expected systematic measurement error of the system, which includes calibration errors, variations in the flow rate during the experiments and the accuracy of the rotameter. The standard deviation of the velocities at the centerline is 7.9 mm/s (0.95% of the maximum velocity). This confirms that averaging the results of 100 image pairs is here sufficient to reduce the random measurement errors to within the overall error of the system. Note that the displacement in this case ($\delta = 25$ pixels) was more than a quarter of the final interrogation area size ($\frac{1}{4} \times 8$ pixels). Good results are still obtained despite this large displacement due to the combination of the laminar nature of the flow, iterative analysis scheme and correlation averaging method. The left and right hand side of the flow field still suffer from the large displacement: here tracer particles are entering or leaving the field-of-view. Due to the use of 50% overlap the 5-6 interrogation areas at each end cannot give reliable results. The velocity profiles shown in figure 6, as well as the value of the standard deviation reported earlier, are based on the average of the data from $x = 10$ to $x = 30$ mm.

In the second case, $D = 65$ mm, no useful results can be obtained: there is only a hint of the expected Poiseuille flow pattern (figure 6, bottom contour plot). As can be seen in the right-hand figure, the velocities that are found are significantly lower than the reference values. Note that missing data in the contour plot has been excluded to calculate the velocity profile. Varying the processing parameters (e.g. interrogation area size) did not improve the result.

4.2 Interleaved imaging

Figure 7 shows an image sequence recorded with the new interleaved method. The data shown on the left-hand side represents 4 image pairs, which are recorded with an off-set of $m = 8$. The raw data has here been converted to a B-mode image by taking a Hilbert transform (in the z-direction) and log compression of the intensities for clarity. The middle figure shows a detail of the sequence, clearly showing that the same features are repeated, with an off-set of m. The right-hand figure shows two frames that are obtained after de-interleaving the image sequence. The yellow dots serves as reference mark to indicate the (small) displacement of the contrast medium, in this case approximately 2-3 pixels toward the left.

In figure 8 results are shown for the velocity measurements obtained in the same flow as before, but now using the interleaved method. The left-hand side shows four contour plots of the velocity. All four are obtained at the same frame rate (74 Hz; identical to the second case of the conventional method, as shown in Figure 6 with $D = 65$ mm), but the inter-frame time is chosen different. The value of interleave parameter m was chosen as 7, 15, 31 and 63, which resulted in an effective ΔT of 0.65, 1.51, 3.24 and 6.69 ms (again ignoring the sweep correction). The expected centerline displacements for the four cases are 4, 10, 22 and 45 pixels. As can be seen in the contour plots and the velocity profiles on the right-hand side, the first three cases give good results for the flow field. Note that
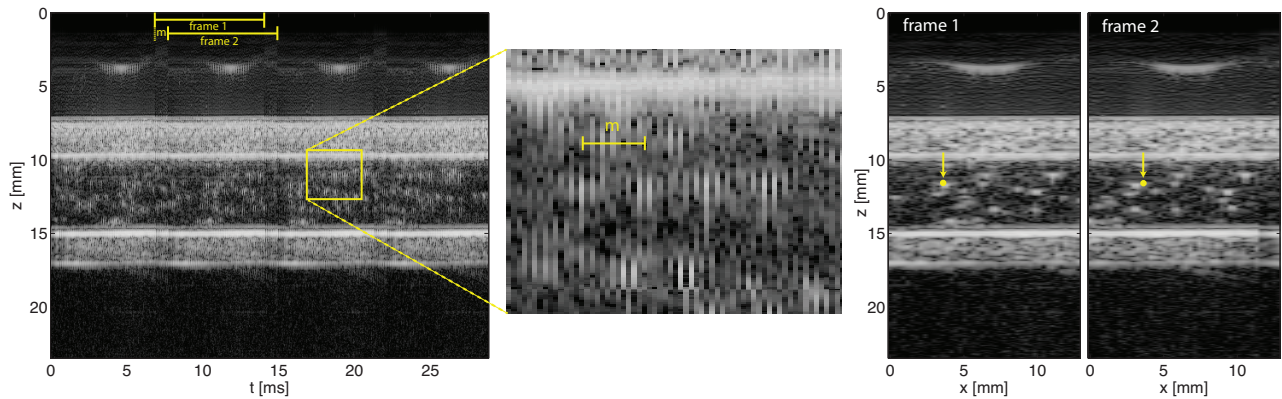
Figure 7: *(Left)* B-mode image sequence recorded using the interleaving method; *(Middle)* Detail of the image sequence; *(Right)* De-interleaved frames.

the displacement for the third case corresponds to that in the first case of the conventional case (D = 25 mm). Using the interleaved method, we are able to measure using a depth of 65 mm. This depth led to unacceptable results in the conventional case. The fourth case of the interleaved study leads to unusable results near the centerline, as could be expected from the displacement predictions (δ = 45 pixels).

To demonstrate the capabilities of the new approach, figure 9 shows measurements using the full field-of-view (L = 3.8 cm) in a flow with a centerline velocity of 1.42 m/s (Re = 1520). The velocity profile with the local standard deviation is shown, together with the reference data (reference centerline value is 1.47 m/s). While it is theoretically possible to measure faster flows with the present hardware and imaging method, practical limitations prevent this with the current flow phantom: the flow will no longer be fully developed and might also become (intermittently) turbulent; this would make it difficult to predict the reference velocity profile from the flow rate only.

5. Discussion

The method introduced in this study enables the variation of the inter-frame time in ultrasound imaging velocimetry, an essential parameter to obtain velocity measurements in a wider dynamic range. The study demonstrates the limitations of the conventional method, for which the maximum measurable velocity is limited by the frame rate that can be achieved. With the interleaved method, higher velocities can be obtained, as shown in figure 9. More importantly, measurements no longer need to be restricted in their field-of-view, as shown in figure 8: these measurements were obtained using the full lateral image width (i.e. all transducer elements) and at an arbitrarily chosen depth. Another advantage of being able to manipulate the inter-frame time is that measurements can be expected to be more accurate. Loss of correlation due to in-plane motion, out-of-plane motion and gradients all scale directly with the inter-frame time (Adrian and Westerweel 2010). Optimization of the inter-frame time is essential to make the transition from measurements of steady flows to instantaneous velocity fields in more complex flows.

### 5.1 Limitations and practical issues

The method uses standard, commercially-available echography equipment. However, it requires low-level access to the transducer imaging read-out protocol. This means that it will currently only be possible to apply it in research-oriented equipment, which is generally more open. A next logical step would be to implement the method into more robust and user-friendly software aimed at clinical use.

One uncertain aspect of the technique is the impact on the sub-pixel accuracy. In conventional PIV, the displacement peak generally has a Gaussian shape (due to the near-Gaussian particle images). In a previous study, we already demonstrated that the the use of standard sub-pixel peak fits in ultrasound imaging velocimetry can lead to inaccurate/biased result (Poelma et al. 2012). A single contrast bubble is much smaller than the transducer pitch and its projected lateral beam width. However, contrast bubbles echoes still create an 'image' that covers multiple lines (see e.g. figure 7). Nevertheless, one could argue that the interleaved imaging could introduces additional artifacts. These were not observed in the present experiments. It is expected that they are largely diminished due to averaging effects; correlation results are here averaged in time, but also spatially due to the finite window size.

A final drawback can result from the interplay between tracer displacement and the interleaved off-set. This is demonstrated in figure 10 for a case with a very large tracer displacement. An inter-frame time of ΔT = 19.6 ms, equivalent 51 Hz, would result in a displacement of approximately 99 pixels at the centerline with the conventional method. Here, the flow is measured using an interleaved off-set of m = 15. This results in an uncorrected displacement field where the near-wall regions appear to move in the opposite direction compared to the centerline region (see figure 10). Note that this is simply a result of the interleaved method, which can be interpreted as a simultaneous spatial and temporal shift. As long as the proper local ΔT is used (as given by equations 1 and 2), the displacement field still leads to the expected velocity profiles; the local ΔT (the denominator in equations 1 and 2) changes sign at the same moment
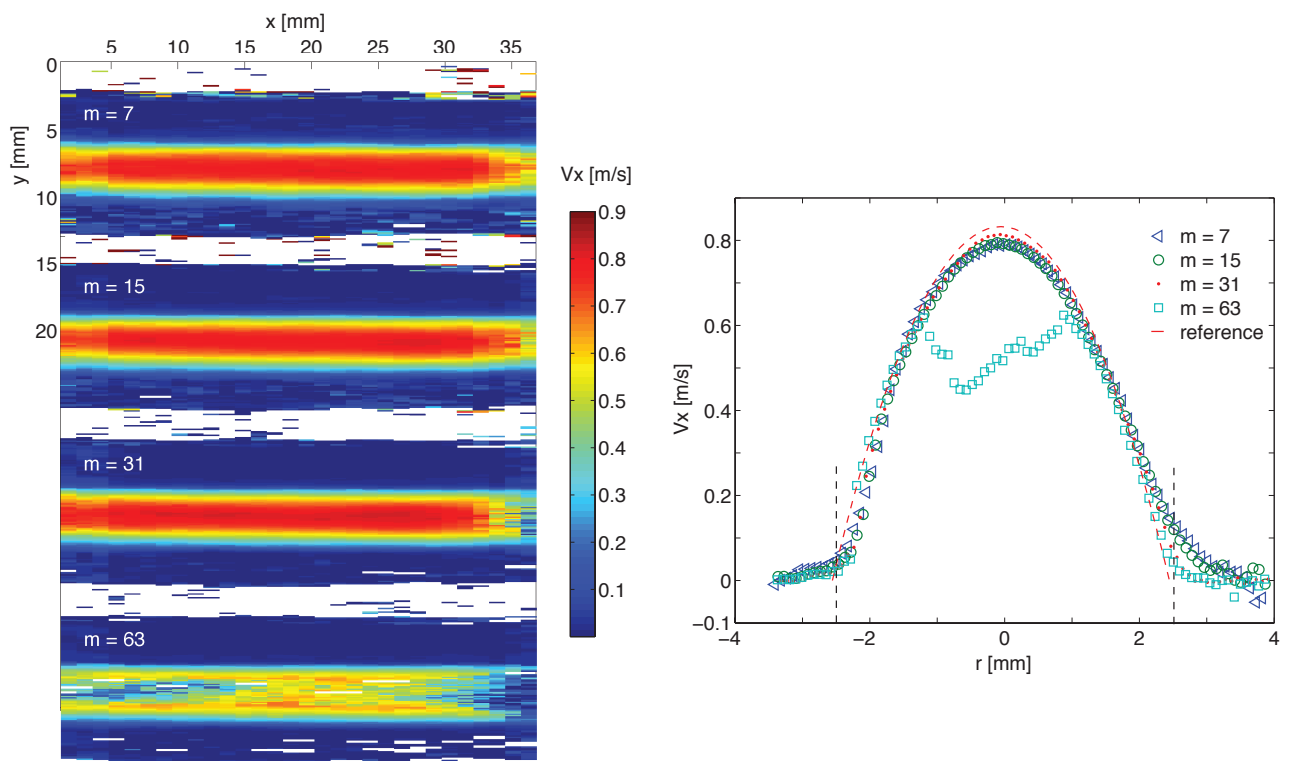
Figure 8: *(Left)* Results using the interleaved method for a constant flow (same as previous figure; $D = 65$ mm) and frame rate, but with increasing interleaved off-set m. *(Right)* Velocity profiles and reference.
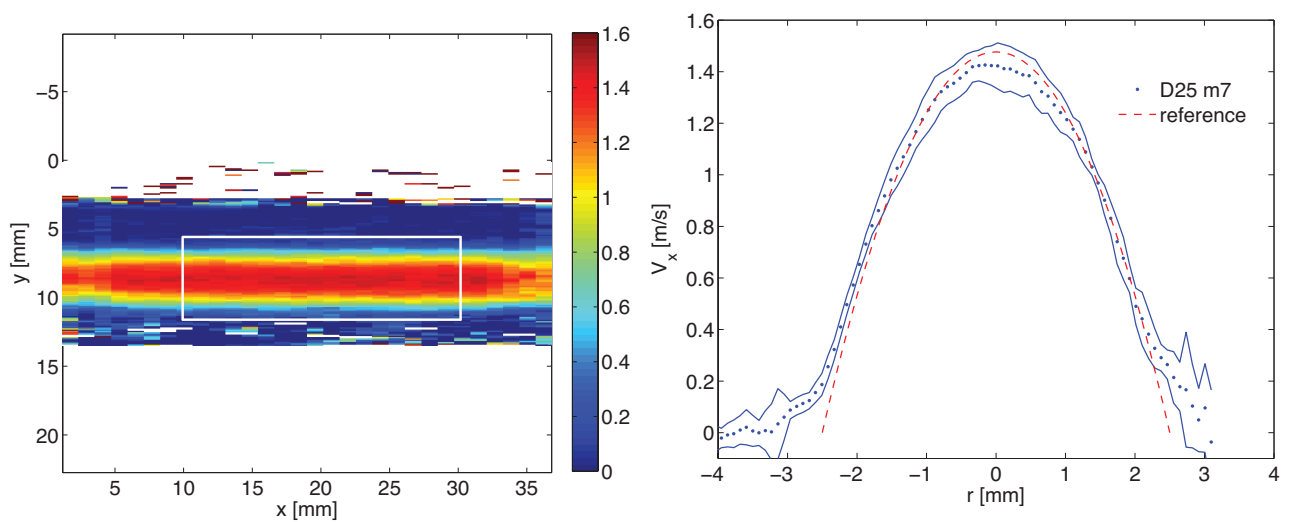
Figure 9: *(Left)* Interleaved results for a flow beyond the capabilities of the conventional method. Imaging depth $D = 25$ mm, off-set $m = 7$. *(Right)* Velocity profiles and standard deviation (averaged along line 10-30, as shown by the white rectangle).
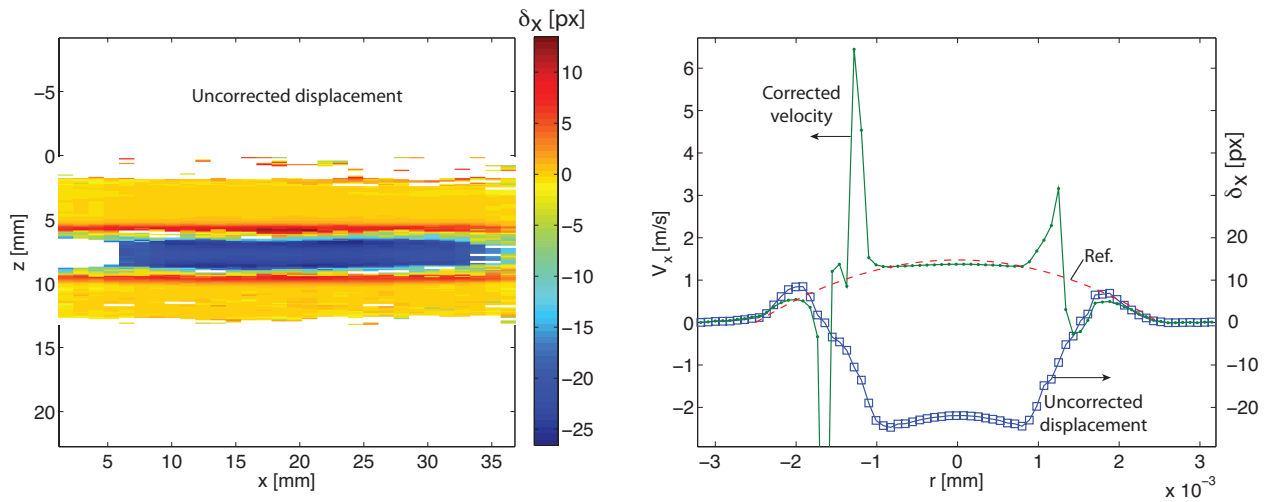
Figure 10: *(Left)* Uncorrected displacement field *(Right)* Uncorrected displacement profile, corrected velocity profile and reference velocity profile.

as the displacement (numerator) changes sign. However, at the radial position where ΔT changes sign, the velocity estimate becomes unreliable: the displacement is divided by a (very) small number so that noise will blow up (see right-hand side of figure 10). This can be avoided by choosing the measurement parameters, in particular m and sweep direction, so that the denominators of equations 1 and 2 do not approach zero. Notice that the erroneous velocities are found around when the sum of uncorrected displacement and the interleaved off-set ($m = 15$) approaches zero.

6. Conclusion and Outlook

In this study, we introduce a novel imaging method that enhances the dynamic range of ultrasound imaging velocimetry by an interleaved read-out approach. This means that the inter-frame time is no longer fixed to the imaging rate. In particular, this means that the displacement of fast flows can be reduced by choosing the appropriate image off-set parameter m. We show that it is therefore now possible to measure flows up to 1.4 m/s with the maximum lateral field-of-view and (relatively) unrestricted depth. Such measurements have not been reported before, as the conventional methods could not capture such fast flows. Faster flows are measurable in theory; the flow phantom is here the limiting factor.

The use of interleaved imaging makes the use of the sweep-correction even more critical than in conventional ultrasound imaging velocimetry applications, as the effective imaging rate is doubled and generally the full image width will be utilized. While the distorted velocity field can be corrected easily, one has to be careful in choosing measurement parameters: it should be avoided that the off-set balances the local tracer displacement, as noise levels can then increase dramatically.

Current experiments are performed in a steady, laminar flow. With the introduction of the inter-frame time, it may become possible to start evaluating instantaneous flows in more interesting flows. The study of 'disturbed' flows in more complex cases (e.g. an aortic arch flow phantom), and ultimately in vivo flows, is part of ongoing studies. The ability to freely choose the inter-frame time will be essential to obtain results in these flows. Apart from moving from time-averaged flows to instantaneous flow measurements, it might also be possible in the future to capture three-dimensional flows. Three-dimensional ultrasound imaging is rapidly developing, but the even lower imaging rates have so far prohibited flow measurements - unless steady flow fields are reconstructed slice by slice (Poelma et al. 2011b). The present interleaved approach can be extended to two-dimensional transducers.

Ultrasound imaging velocimetry is a promising new method for measuring blood flow. However, in order to truly fulfill the potential for the technology, it is important that the methodology is optimized as a whole, rather than taking advantage of piecemeal existing methods. With the present paper, we have given an example of this approach: rather than re-use existing read-out methodologies aimed at *imaging*, we devised a novel read-out method for *velocimetry*. This will increase the potential of ultrasound imaging velocimetry in clinical settings.

REFERENCES

Adrian R.J. and Westerweel J. : 2010, *Particle Image Velocimetry*, Cambridge University Press, United Kingdom.

Beulen B. , Bijnens N. , Rutten M. , Brands P. and van de Vosse F. : 2010, Perpendicular ultrasound velocity measurement by 2D cross correlation of RF data. Part A: validation in a straight tube, *Experiments in fluids* **49**(5), 1177–1186.

Hill C.R. , Bamber J.C. and Ter Haar G. : 2004, *Physical principles of medical ultrasonics*, Wiley Online Library.

Hong G.R. , Pedrizzetti G. , Tonti G. , Li P. , Wei Z. , Kim J.K. , Baweja A. , Liu S. , Chung N. , Houle H. et al.: 2008, Characterization and Quantification of Vortex Flow in the Human Left Ventricle by Contrast Echocardiography Using Vector Particle Image Velocimetry, *JACC: Cardiovascular Imaging* **1**(6), 705–717.

Hoskins P.R. : 2010, Haemodynamics and blood flow measured using ultrasound imaging, *Proceedings of the Institution of Mechanical Engineers, Part H: Journal of Engineering in Medicine* **224**(2), 255–271.

Kheradvar A. , Assadi R. , Falahatpisheh A. and Sengupta P.P. : 2011, Assessment of transmitral vortex formation in patients with diastolic dysfunction, *Journal of the American Society of Echocardiography* **25**, 220–227.

Kheradvar A. , Houle H. , Pedrizzetti G. , Tonti G. , Belcik T. , Ashraf M. , Lindner J.R. , Gharib M. and Sahn D. : 2010, Echocardiographic particle image velocimetry: a novel technique for quantification of left ventricular blood vorticity pattern, *Journal of the American Society of Echocardiography* **23**(1), 86–94.

Kim H.B. , Hertzberg J.R. and Shandas R. : 2004, Development and validation of echo PIV, *Experiments in Fluids* **36**(3), 455–462.

Montaldo G. , Tanter M. , Bercoff J. , Benech N. and Fink M. : 2009, Coherent plane-wave compounding for very high frame rate ultrasonography and transient elastography, *Ultrasonics, Ferroelectrics and Frequency Control, IEEE Transactions on* **56**(3), 489–506.

Poelma C. , Mari JM , Foin N. , Tang M.X. , Krams R. , Caro CG , Weinberg PD and Westerweel J. : 2011b, 3d flow reconstruction using ultrasound piv, *Experiments in fluids* **50**(4), 777–785.

Poelma C. , van der Mijle R.M.E. , Mari J.M. , Tang M.X. , Weinberg P.D. and Westerweel J. : 2012, Ultrasound imaging velocimetry: Toward reliable wall shear stress measurements, *European Journal of Mechanics-B/Fluids* **35**, 70–75.

Poelma C. , Vennemann P. , Lindken R. and Westerweel J. : 2008, In vivo blood flow and wall shear stress measurements in the vitelline network, *Experiments in Fluids* **45**(4), 703–713.

Sengupta P.P. , Khandheria B.K. , Korinek J. , Jahangir A. , Yoshifuku S. , Milosevic I. and Belohlavek M. : 2007, Left Ventricular Isovolumic Flow Sequence During Sinus and Paced Rhythms New Insights From Use of High-Resolution Doppler and Ultrasonic Digital Particle Imaging Velocimetry, *Journal of the American College of Cardiology* **49**(8), 899–908.

Taylor C.A. and Draney M.T. : 2004, Experimental and computational methods in cardiovascular fluid mechanics, *Annu. Rev. Fluid Mech.* **36**, 197–231.

Van Ooij P. , Guédon A. , Poelma C. , Schneiders J. , Rutten M.C.M. , Marquering H.A. , Majoie C.B. , Van Bavel E. and Nederveen A.J. : 2012, Complex flow patterns in a real-size intracranial aneurysm phantom: phase contrast mri compared with particle image velocimetry and computational fluid dynamics, *NMR in Biomedicine* **25**(1), 14–26.

Westerdale J. , Belohlavek M. , McMahon E.M. , Jiamsripong P. , Heys J.J. and Milano M. : 2011, Flow velocity vector fields by ultrasound particle imaging velocimetry, *Journal of Ultrasound in Medicine* **30**(2), 187.

Zhang F. , Lanning C. , Mazzaro L. , Barker A.J. , Gates P.E. , Strain W.D. , Fulford J. , Gosling O.E. , Shore A.C. , Bellenger N.G. et al.: 2011, In vitro and preliminary in vivo validation of echo particle image velocimetry in carotid vascular imaging, *Ultrasound in medicine & biology* **37**(3), 450–464.

Zheng H. , Liu L. , Williams L. , Hertzberg J.R. , Lanning C. and Shandas R. : 2006, Real time multicomponent echo particle image velocimetry technique for opaque flow imaging, *Applied Physics Letters* **88**, 261915.

Zhou B. , Fraser K.H. , Poelma C. , Mari J.-M. , Eckersley R.J. , Weinberg P.D. and Tang M.-X. : in print, Ultrasound imaging velocimetry: effect of beam sweeping on velocity estimation, *Ultrasound in Medicine and Biology* .